Electric Field Enhanced Electroluminescence Color Tuning of Colloidal Type-II Tetrapods

Chenghao Wang[1#], Jianhui Fu[2#], Qi Wei[1,2#], Hui Ren[1], Qi Liu[1], Luwei Zhou[1], Pengzhi Wang[1], Mingjie Li[1,2,3]*

1. Department of Applied Physics, The Hong Kong Polytechnic University, Hung Hom, Kowloon, Hong Kong, China

2. Shenzhen Research Institute, The Hong Kong Polytechnic University Shenzhen, Guangdong, 518057, China

3. Photonics Research Institute, The Hong Kong Polytechnic University, Hung Hom, Kowloon, Hong Kong, China

[*] E-mail: ming-jie.li@polyu.edu.hk

KEYWORDS: colloidal nanostructures; type-II band alignment; EL color tuning; carrier dynamics

Abstract

Color-tunable electroluminescence (EL) from a single emitting material can be used to develop single-pixel multicolor displays. However, finding materials capable of broad EL color-tuning remains challenging. Herein, we report the observation of broad voltage-tunable EL in colloidal type-II InP/ZnS quantum dot-seeded CdS tetrapod (TP) LEDs. The EL color can be tuned from red to bluish-white by varying the red and blue emission intensities from type-II interfaces and arms, respectively. The capacitor device proves that an external electric field can enhance the color-tuning in type-II TPs. COMSOL simulations, numerical calculations, and transient absorption measurements are performed to understand the underlying photophysical mechanism. Our results indicate that the reduced hole relaxation rate from the arm to the quantum dot core can enhance the emission from the CdS arms, which is favorable for EL color-tuning. This study provides a novel method to realize voltage-tunable EL colors with potential in display and micro-optoelectronic applications.

Main Text

The conventional full-color light-emitting diodes (LEDs) are limited by the requirement of multiple subpixels that emit colors such as red, green, and blue.[1] Single-pixel color-tunable LEDs have attracted increasing interest for novel display and optoelectronic applications owing to their improved pixel resolution and reduced fabrication complexity and cost.[2-5] The proposed methods to achieve electroluminescence (EL) color-tuning in organic and/or inorganic LEDs typically include voltage-dependent energy transfer from the low emission–energy host to the high emitting–energy dopant in organic materials and vertical stacking of multiple active components that emit independently at different wavelengths when activated at different current injection levels.[6-13] However, the reported color-tuning range of voltage-dependent energy transfer is usually narrow because it is limited by the available material types. Furthermore, vertical stacking of multiple active components requires sophisticated fabrication techniques to ensure the different color-emitting components (e.g., red-, green-, and/or blue-emitting quantum dots (QDs) or polymers) are correctly positioned and individually controlled. Therefore, finding a new strategy to fabricate a single-emissive material capable of wide EL color-tuning remains challenging.

Colloidal semiconductor nanostructures have been utilized as chromophores in new-generation LEDs owing to their high-yield fabrication via wet chemical methods, spectrally narrow emission profiles, and ability to tune color by changing the crystal size or composition.[14-20] Developing colloidal heterostructures with multiple emitting states is a desirable method for creating full-color light sources. For example, dual-wavelength photoluminescence (PL) and EL have been achieved with distinct emission colors from the respective core and shell in type-I

CdSe QD-seeded CdS tetrapods (TPs)[21, 22] and CdSe/CdS dot-in-bulk QDs.[23, 24] However, using these type-I heterostructure systems for emission color is inappropriate because EL intensities of both components from QD core and shell scale equally under an applied bias.[22,24]

To achieve a wide EL color–tuning range, there should be a large energy difference between photon energies from different emission states and emission intensities of different colors should be easily and gradually tunable. Semiconductor heterostructures with a type-II alignment can meet these criteria because (i) the emission energy of type-II interface is much smaller than the bandgaps of the two components of heterostructure and (ii) the interface emission is saturated at high carrier densities because of the long-lived excited state, thereby facilitating the recombination of high-energy excitons in the heterostructure. Our previous study reported on the wide PL color-tuning from red to blue in InP/ZnS core–shell QD-seeded CdS type-II TPs at low-to-high optical excitations.[25] Therefore, type-II TPs may be a new candidate for the development of color-tunable LEDs. Importantly, different from PL, the active layer of an LED is exposed to high electric fields during operation. The electric field in the LED device can trigger new EL color–tuning behavior in type-II heterostructures, which has rarely been investigated.

Herein, the first color-tunable EL using colloidal type-II heterostructures of InP/ZnS QD-seeded CdS TPs is achieved, where the EL color can be changed from red to bluish-white by adjusting the applied voltage. The color can be tuned because of the difference in the intensities between the spectrally distinct emission from the red-emissive type-II QD/arm interfaces and blue-emissive CdS TP arms. Electric field–dependent PL and carrier dynamics measurements and electron wavefunction redistribution calculations under an electric field show that the incorporation of an electric field in type-II TP can effectively reduce the hole-localization rates.

This reduction is beneficial for observing the CdS arm emission typically seen at high carrier densities, thereby increasing the color variability of EL. These findings suggest that colloidal type-II semiconductor heterostructures can afford solution-processed LEDs with wide emission color tunability.

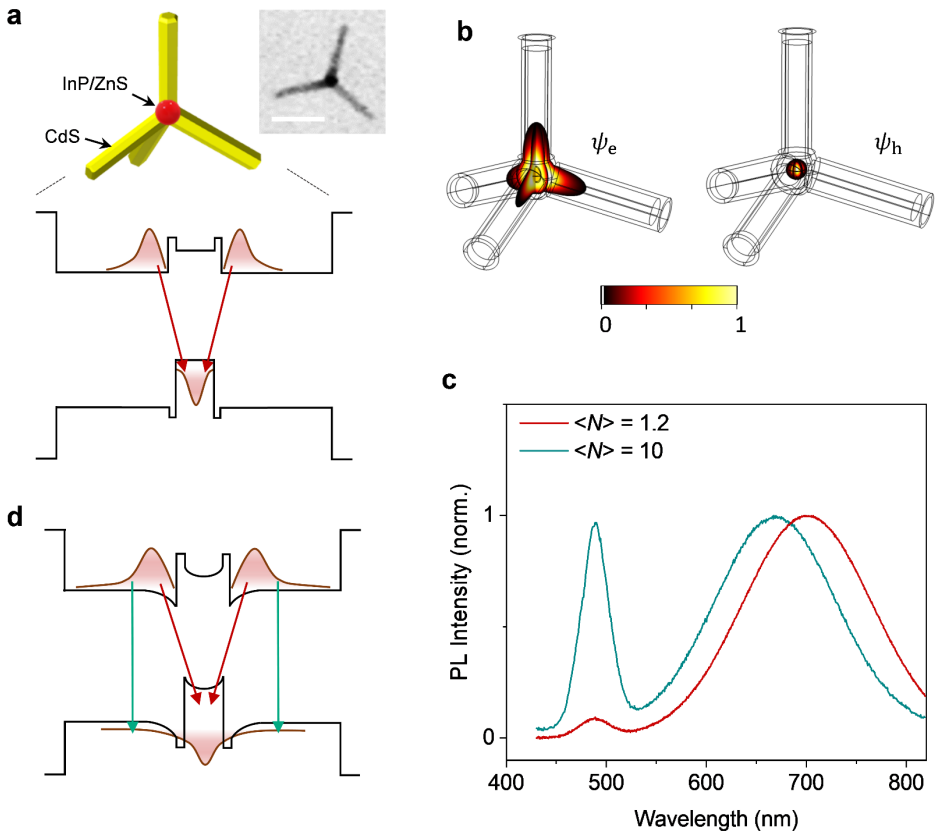

Figure 1. Structural characterization and optical properties. (a) TEM image and schematic of an InP/ZnS QD-seeded CdS TP and schematic representation of electron and hole wavefunction distributions in the conduction and valence bands along the core and one of the Cds arms. Scare bar: 20 nm. (b) Calculated electron and hole wavefunction distributions in the TP using COMSOL multiphysics simulation. (c) Normalized PL spectra of a TP film at low and high pump fluences. (d) Schematic representation of band bending at high carrier densities.

Our InP/ZnS core–shell QD core-seeded CdS TPs were synthesized by a hot-injection method with PL quantum yield (PLQY) of 22±3% (see details in the Supporting Information). The QD core of the TP has a diameter of ~3 nm with an arm diameter of 5 nm and a length of 28 nm (Fig. S1). Figure 1a shows the schematic structure of a TP and type-II band alignment, in which holes are localized in the QD core and electrons predominantly reside in the CdS arms near the QD/arm interfaces, as demonstrated by the calculated electron (ψ_e) and hole (ψ_h) wavefunction distributions (Fig. 1b). The dual-wavelength PL behavior of a spin-coated TP thin film was characterized. The average number of electron–hole pairs per TP ($\langle N \rangle = J \times \sigma$) is controlled by pump fluence J and determined absorption cross-section σ of 7×10^{-14} cm^{-2} (Fig. S2). Under an excitation of $\langle N \rangle = 1.2$, red emission (centered at ~695 nm) from the type-II QD/arm interface is dominant, as shown in Fig. 1c. Because CdS arms have a much larger volume than the core, most of the electron–hole pairs are initially generated in the TP arms. The holes in the CdS arms then localize to the core because of the thermodynamic driving force caused by the large valence band offset between InP and CdS, and electrons move to the interfaces by Coulomb interactions. The efficient transfer of holes from the arms to core of the TP explains why type-II emission, resulting from the recombination of electron–hole pairs across the QD/arm interface, is dominant at low injection densities. To observe the blue emission of the CdS arm at ~486 nm and tune the overall emission color of the TP, a much higher carrier injection density is required. As shown in Fig. 1c, a considerable CdS emission emerges only at a transient pump intensity with an $\langle N \rangle$ of ~10. At such high carrier densities, the hole states in TP QD-cores are saturated, reducing the driving force for holes to relax into the core because of the exciton blocking effect, as previously observed in CdSe QD-seeded CdS TP.[21, 23] The blue shift of the interface emission peak with an

increase in optical excitation intensity is because of the unique band bending (Fig. 1d) arising from the high concentration of separated opposite charges at the type-II interfaces.[26-29]

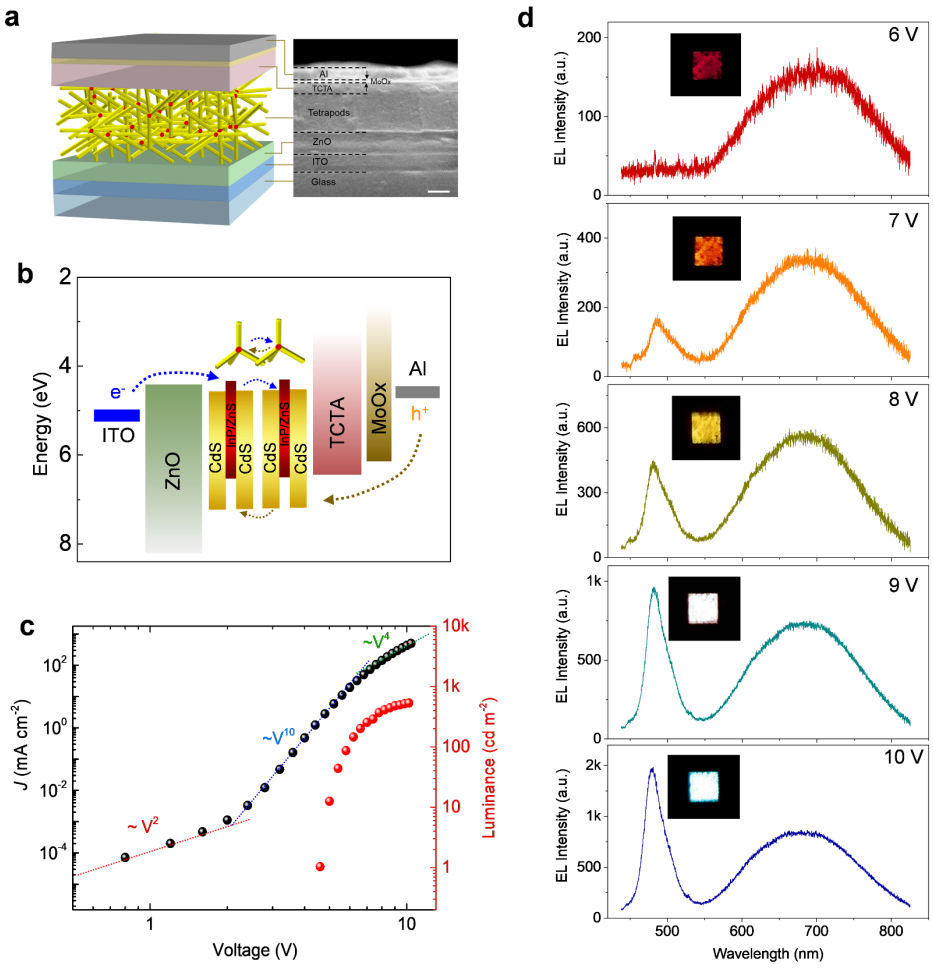

Figure 2. Structure and voltage-tunable EL spectra of the TP-LED. (a) Schematic illustration (left) and a cross-sectional SEM image (right) of the TP-LED in an inverted device structure. Scale bar: 50 nm. (b) Energy band diagram of the TP-LED with an inverted device architecture. The energy levels of TPs were determined using ultraviolet photoemission spectroscopy (UPS) and UV–visible measurements and other functional layers were obtained from refs.[30, 31] (c) Log–log plots of current density–voltage (*J*–*V*) and luminance–voltage. Power law-fitting of the *J*–*V* curve reveals three different conduction regimes with transitions from a space-charge limited to a high- and low-density trap-limited conduction regimes. (d) EL spectra at different applied

voltages. Insets show the photographs of the TP-LED with an active area of ~1 × 1 mm^2 under different forward biases.

To investigate the possibility of tuning the EL color with the dual-emitting type-II TPs, an LED device was fabricated using an inverted architecture, as shown in Fig. 2a. Indium tin oxide (ITO) was used as the cathode, and a spin-coated ZnO nanoparticle thin film (~20 nm thick) is used as the electron-transport layer. The TP solution was spin coated onto the ZnO nanoparticle layer, affording an active layer with a thickness of ~100 nm. A thin layer of Al was used as the anode, and tris(4-carbazoyl-9-ylphenyl)amine (TCTA, ~50 nm thick) and molybdenum oxide (MoOx; ~10 nm) were employed as the hole-transport layers. The energy-level diagram of the LED device is shown in Fig. 2b, wherein the work functions of the different layers are based on literature values.[30, 31] Since the TPs are comprising ligands with long alkyl chains, the mechanism of charge transport across the thick layer of TPs is probably carrier tunneling and/or field-assisted hopping between TPs, similar to that in colloidal QDs. Fig. 2c shows the current density versus voltage (*J*–*V*) log–log plot under a forward bias for the TP-LED device. When the applied voltage is < 2.0 V, the increase in current density *J* with V^2 indicates space charge–limited conduction.[14] The increase in the *J*–*V* slope to 10 under the voltage higher than 2.0 V is attributed to trap-limited conduction, which is associated with the onset of electron and hole injections into the TPs. In this regime, TPs behave as charge-trap sites. At an applied voltage > 7.0 V, the subsequent decrease in the *J*–*V* slope is because of the saturation of the excited states in some TPs at larger current densities. The LED device exhibits a peak external quantum efficiency (EQE) of ~1.6% and good stability at a current density of 22 mA cm^{-2} (Fig. S3).

Figure 2d shows a series of EL spectra and associated photographs of the device operating under an applied forward bias of 6.0–10.0 V, which demonstrate the wide range of colors from

red to bluish white. At an applied voltage < 6.0 V, the EL spectrum exhibits a broad band centered at ~700 nm from the type-II core–arm interface. As the voltage bias increases, a bluish-green EL band centered at ~480 nm is observed and its intensity increases quickly compared to that of the initially dominant red emission. Based on its spectral shape and peak position, the bluish-green emission is from the recombination in the CdS arms of the TPs, rather than from the ZnO (centered at ~380 nm) or TCTA (centered at ~410 nm[32]) layers. The difference in the intensity of red and bluish-green ELs at different biases accounts for the overall effective and gradual color change.

The TPs EL spectra show a similar trend of color tuning as observed in the PL spectra under high-intensity excitation (Fig. 1c). However, note that the electrical excitation in the LED is several orders of magnitude smaller than that under the fs-laser pulse excitation. For example, at a current density of 550 mA cm^{-2} and 10 V in the LED, the nominal number of injected electron–hole pairs per TP is estimated to be ~ 0.6, which is estimated using $\langle N \rangle = \frac{Jv}{qd}\tau$, where q is the charge, d is the thickness of the TP layer, v is the volume of the TP, and τ carrier recombination lifetime determined from PL lifetime (Fig. S2). Such low carrier density thus indicates to achieve CdS arm EL for the color tuning is much easier under conditions of electrical injection than that of PL which requiring much higher injected carrier densities (e.g., $\langle N \rangle$ ~ 10 in Fig. 1c).

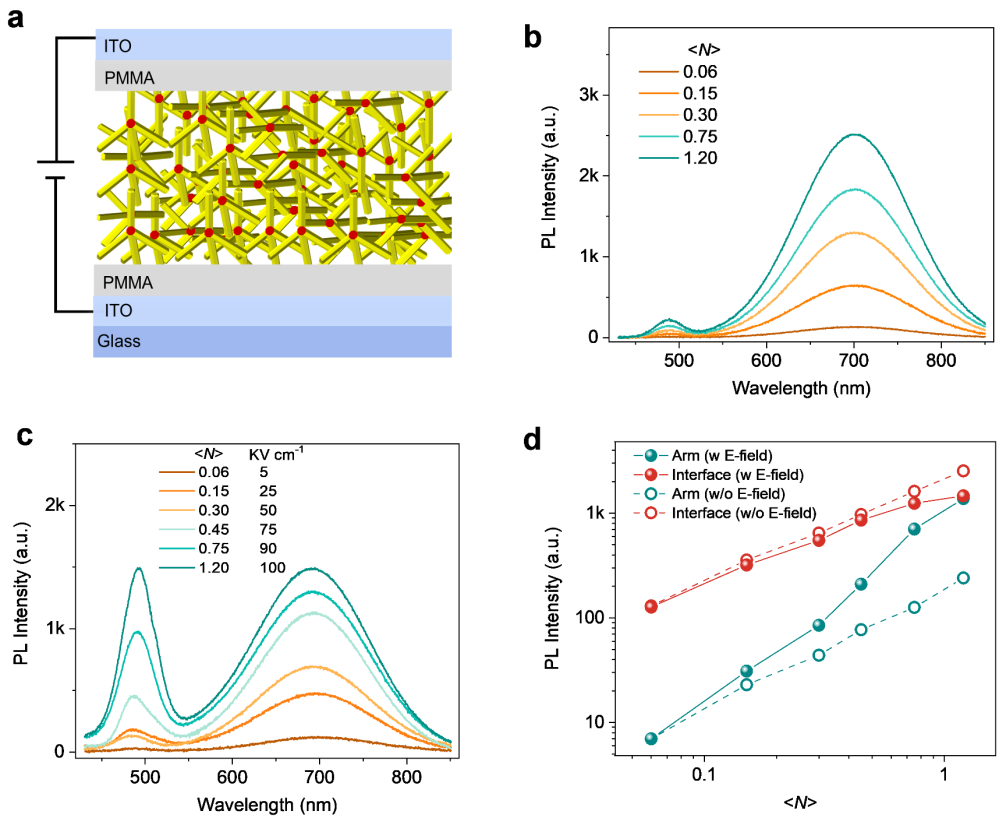

Figure 3. Effect of electric field on emission spectra of TPs. (a) Schematic illustration of the TP-based capacitive device. PL spectra of the TP-capacitive device under different <*N*> (photoexcited electron-hole pair numbers per TP) (b) without an electric field and (c) with different electric fields. (d) CdS arm (green) and QD/arm interface (red) PL intensities as a function of <*N*> without (opening circles) and with (solid dots) electric field (E-field) obtained from PL spectra in (b) and (c).

During the operation of the TP-LED device, the emissive TP layer experiences an effective electric field of ~10^2 KV cm^{-1} (estimated based on the distance between the two electrodes of LED). Previous studies have reported that an electric field can modulate the emission wavelength and intensity of type-II nano-heterostructures due to the quantum-confined Stark effect (QCSE).[33-35] To understand the effect of the electric field on the EL color–tuning properties of our TPs, the PL of a TP film (~100 nm thick, the same thickness as in the LED) sandwiched

between PMMA/ITO transparent electrodes under an applied voltage is investigated (Fig. 3a). This structure allows the application of an electric field across the TP film without inducing charge injection. The leakage current density of our capacitive device is as low as ~10^{-6} A cm^{-2} under an applied bias of 10 V (Fig. S4), indicating that the charge injection is negligible.

In the absence of an electric field, the two emission bands linearly increase with an increase in power of the optical pump (Fig. 3b). At a fixed optical excitation intensity, as the strength of the electric field increases, the emission from the interface decreases whereas that from the CdS arms increases (Fig. S5a). Additionally, the CdS arm and QD/arm type-II interface emission peaks slightly redshifts with increasing electric field due to the QCSE, which is also reflected by the electro-absorption measurement (Fig. S5b). The quenching of interface emission and simultaneous enhancement in arm emission indicate an increased probability of electron–hole pairs in the CdS arms with increasing electric field. In the LED, as the applied voltage increases, the injected carrier density and electric field in the TP film increase. To demonstrate the optical properties of the TP film in a similar situation with existence of electric field to that in the LED, the PL spectra of TPs were measured at increasing carrier densities and electric fields simultaneously. As shown in Fig. 3c and 3d, the emission of the CdS arm becomes more prominent in the presence of an electric field. Furthermore, no emission was observed with applied voltages only and without photoexcitation, indicating that the electric field–induced emission makes a negligible contribution to the EL and PL of TPs. The trends observed in the PL spectra evolution of TPs in capacitor are also reproducible. These results show that the presence of an electric field in an LED significantly promotes the emission of the CdS arm and improves the color tunability of type-II TPs.

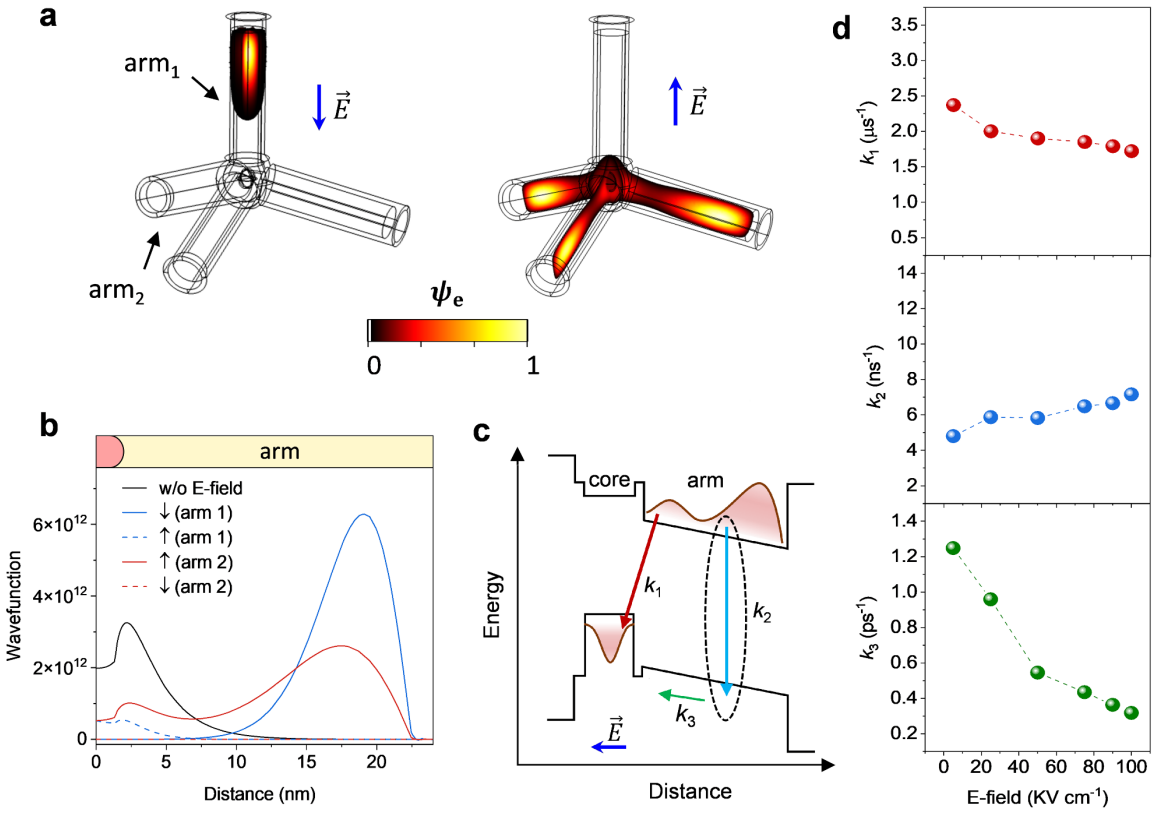

Figure 4. Effect of electric field on emission spectra of TPs. (a) Electron wavefunction distributions under electric-field at two opposite directions calculated by COMSOL multiphysics simulation. (b) Electron wavefunction distribution profiles of the representative CdS arms in (a) without and with electric fields at two opposite directions. (c) Schematic energy-level diagram of TP in the presence of an external electric field together with carrier dynamic processes. (d) Calculated carrier recombination and relaxation rates k_1, k_2 and k_3 under different electric fields.

The electron and hole wavefunction distributions are simulated to quantitatively understand the mechanism behind the enhanced emission of the CdS arm in the presence of an electric field. Since the TPs are randomly arranged in the film, the electron wavefunction distributions in TPs were calculated under opposite directions of the electric field along the CdS arm as two extreme conditions. Figure 4a shows that regardless of the direction of the electric field, the electron

wavefunctions (originally localized near the core–arm interfaces as shown by black lines in Fig. 4b) move to the TP arms, while holes are still localized in the QD core (Fig. S6). Figure 4c shows the schematic energy-level diagram and electron–hole wavefunction distributions in the presence of an external electric field together with three critical processes on dual emissions. After photoexcitation, the initially photoexcited holes in CdS arms relax into QD-core with nonradiative rate of k_3, followed by the electron-hole radiative recombination with rates of k_1 for type-II interface emission and k_2 for CdS arm emission, respectively. Because of the distributed electron wavefunctions in the CdS arms in the presence of an electric field, after photoexcitation, the driving force for hole localization to the QD core would be reduced by the Coulomb interaction from the electrons in the CdS arms, reducing the hole-localization rate to the core. Therefore, the electron–hole recombination probability in the arm increases, promoting the emission of the CdS arm emission in the presence of an electric field.

A rate equation model considering three dynamics processes (Supplementary Note 1) is used to extract the recombination rates from the experimental measured power-dependent PL intensities in the presence and absence of an electric field (Fig. 3d). As shown in Fig. 4d, as the strength of the electric field increases, interface recombination rate k_1 decreases and k_2 increases slightly. Such variation trends of k_1 and k_2 in the presence of an electric field are also consistent with the time-resolved PL results (Fig. S7). The decreased k_1 can be understood due to the QCSE and increased k_2 would be mainly because of the enhanced probability of excitons inside the CdS arms under electric field. In contrast, there is an obvious decrease in the localization rate k_3 from 1.25 to 0.3 ps^{-1} with increasing electric field, which is consistent with our above analysis from wavefunction distributions.

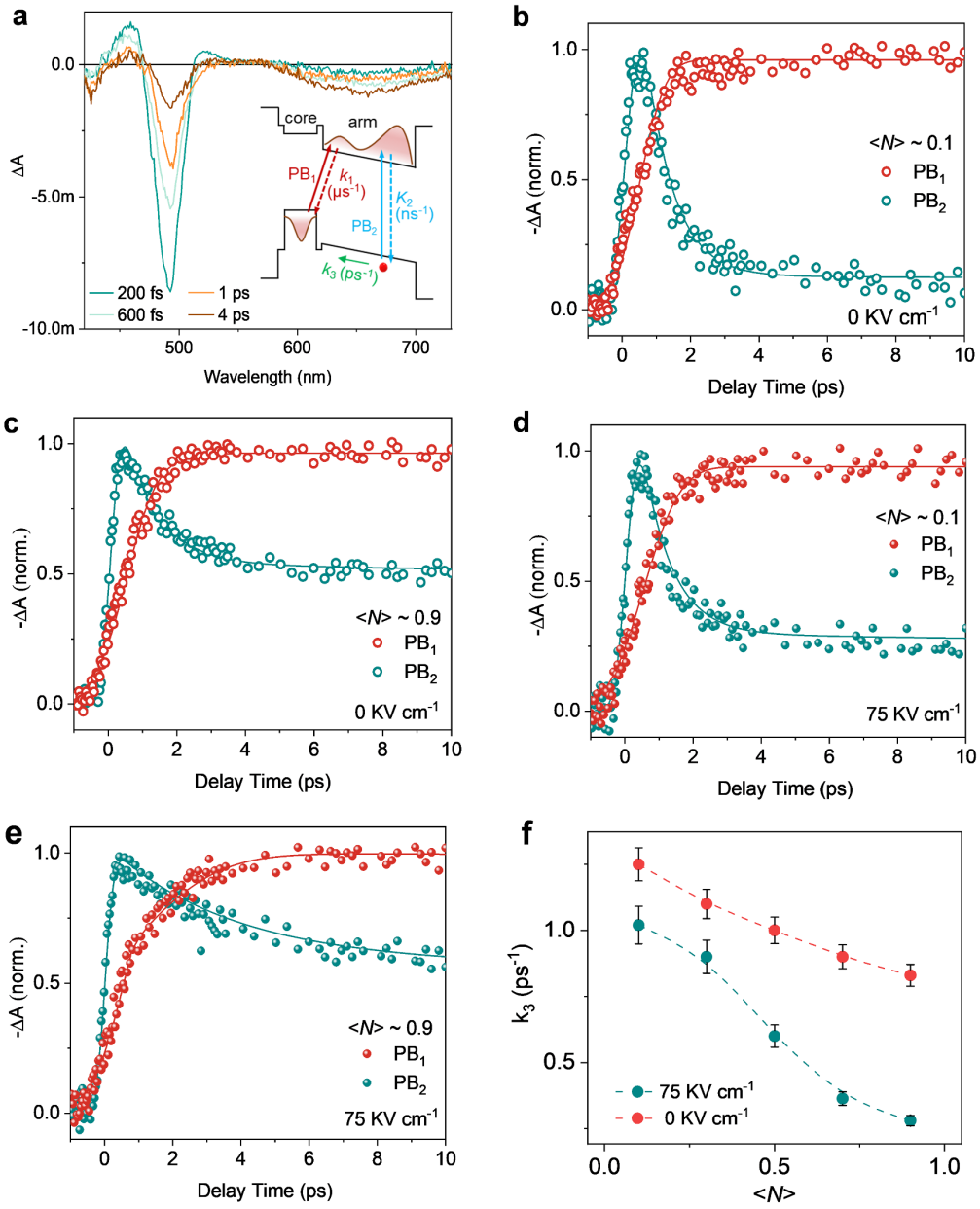

Figure 5. Carrier localization in TPs in the presence of an electric field. (a) TA spectra of the TPs under 400-nm fs laser excitation with 75 KV cm^{-1} electric field. TA dynamics probed at the transitions of the type-II QD/arm interface (red dots) and CdS arms (green dots) in the (b) (c) absence and (d) (e) presence of an electric field under different pump fluence of $\langle N \rangle$ = 0.1 and 0.9, respectively. Solid lines are bi-exponential decay fittings. (f) Fitted hole-relaxation rate k_3 as a function of $\langle N \rangle$.

To further confirm the calculation results of the reduced nonradiative hole-localization rate (k_3) in the presence of an electric field (which cannot be directly determined by time-resolved PL spectroscopy), femtosecond transient absorption (TA) spectroscopy was applied on the above TP capacitor under transmission geometry. TA spectra exhibit a sharp photobleaching (PB) peak PB_2 at 490 nm corresponds to a CdS arm transition and a weak broad band PB_1 with a peak position at ~650 nm corresponds to the type-II transition (Fig. 5a). At a low pump fluence of $\langle N \rangle \sim 0.1$ without electric field, there is a fast decay for the PB_2 band with a rate of 1.5 ps^{-1} (Fig. 5b). Such decay process corresponds to a slow rise probed at PB_1 band with a close lifetime, which is due to the hole relaxation from CdS arm to the QD-core with rate of k_3. The large amplitude of ~85% of this fast decay indicate that most of the holes in CdS arm are localized into the TP core, and thus the interface emission dominates. As the pump fluence increases up to $\langle N \rangle \sim 0.9$, the hole localization decreases to 0.7 ps^{-1} because of the Coulomb blockade effect caused by the filling of core states (Fig. 5c). Interestingly, in the presence of an electric field of 75 KV cm^{-1}, it is found that the rate k_3 become smaller and decreases more rapidly. It decreases from 1.1 ps^{-1} with an amplitude of ~72% under $\langle N \rangle \sim 0.1$ to 0.26 ps^{-1} with amplitude of ~35% under $\langle N \rangle \sim 0.9$ (Fig. 5d, 5e). The smaller and faster declined k_3 values under electric field (Fig. 5f) is well consistent with the predictions in Fig. 4d. The smaller amplitudes of k_3 in the presence of an electric field also indicate more holes remain in CdS arm after photoexcition. These results thus confirm the reduced hole-localization rate in the presence of an electric field and indicate that the reduced hole-localization rate from CdS arm to the core enhance the CdS arm emission is the reason to achieve the easier EL color-tuning under electric field.

In conclusion, we achieved color-tunable LED using colloidal type II TPs as the emissive layer. The EL is tunable by varying the red emission from the QDs/arm interface and bluish-

green emission from the CdS arms of the TPs at different voltages. The mechanism of efficient color tuning is investigated by applying an electric field to the TP film in a TP-capacitive device. From the numerical simulation, calculation, and carrier dynamics measurements, it is found that the electric field can significantly promote the CdS arm emission, which is favorable for EL color-tuning, due to the redistribution of the electron wavefunction into the arms and the reduced hole relaxation into the core. Passivation of the TP CdS arms with shell shall be favorable for further improving the device performance (e.g., enhancing the PLQY and EQE) which can be investigated in the future. The results of this study suggest that core-branched type-II semiconductor nano-heterostructures are a promising material for the future development of color-tunable full-color LEDs.

Supporting Information

Further information on the synthesis, device fabrication, experimental details, and the supporting figures is presented. This material is available free of charge via the Internet at.

Author Contributions

C.W., J.F., and Q.W. contributed equally to this work. M.L. conceived the idea and designed the experiments. C.W. performed the sample and device fabrications, characterizations. J.F. contributed simulations and numerical calculations. Q.W. performed the TA and TRPL measurements. H.R. assisted in samples fabrication. Q.L., L.Z. assisted in interpreting the results and drafting the manuscript. All the authors discussed the results and commented on the manuscript at all stages.

Notes

The authors declare no competing financial interest.

Acknowledgments

M.L. acknowledges the financial support from RGC Early Career Scheme (F-PP7Z) and the Shenzhen Science, Technology and Innovation Program (JCYJ20210324131806018).

Reference

1. Schubert, E. F.; Kim, J. K., Solid-state light sources getting smart. *Science* **2005,** *308*, 1274-1278.
2. Berggren, M.; Inganas, O.; Gustafsson, G.; Rasmusson, J.; Andersson, M. R.; Hjertberg, T.; Wennerstrom, O., Light-Emitting-Diodes with Variable Colors from Polymer Blends. *Nature* **1994,** *372*, 444-446.
3. Shen, Z. L.; Burrows, P. E.; Bulovic, V.; Forrest, S. R.; Thompson, M. E., Three-color, tunable, organic light-emitting devices. *Science* **1997,** *276*, 2009-2011.
4. Cheng, G.; Chan, K. T.; To, W.-P.; Che, C.-M., Color Tunable Organic Light-Emitting Devices with External Quantum Efficiency over 20% Based on Strongly Luminescent Gold(III) Complexes having Long-Lived Emissive Excited States. **2014,** *26*, 2540-2546.
5. Hong, Y. J.; Lee, C. H.; Yoon, A.; Kim, M.; Seong, H. K.; Chung, H. J.; Sone, C.; Park, Y. J.; Yi, G. C., Visible-Color-Tunable Light-Emitting Diodes. *Adv Mater* **2011,** *23*, 3284.
6. Krotkus, S.; Kasemann, D.; Lenk, S.; Leo, K.; Reineke, S., Adjustable white-light emission from a photo-structured micro-OLED array. *Light-Sci Appl* **2016,** *5*, e16121
7. Park, S. J.; Song, S. H.; Kim, S. S.; Song, J. K., Charge Modulation Layer and Wide-Color Tunability in a QD-LED with Multiemission Layers. *Small* **2021,** *17*, 2007397.
8. Guo, F.; Karl, A.; Xue, Q. F.; Tam, K. C.; Forberich, K.; Brabec, C. J., The fabrication of color-tunable organic light-emitting diode displays via solution processing. *Light-Sci Appl* **2017,** *6*, e17094.
9. Zhang, J. F.; Ren, B. T.; Deng, S. B.; Huang, J. C.; Jiang, L.; Zhou, D. J.; Zhang, X. L.; Zhang, M.; Chen, R. S.; Yeung, F.; Kwok, H. S.; Xu, P.; Li, G. J., Voltage-Dependent Multicolor Electroluminescent Device Based on Halide Perovskite and Chalcogenide Quantum-Dots Emitters. *Adv Funct Mater* **2020,** *30*, 1907074.
10. Wang, L.; Wang, X.; Bertram, F.; Sheng, B. W.; Hao, Z. B.; Luo, Y.; Sun, C. Z.; Xiong, B.; Han, Y. J.; Wang, J.; Li, H. T.; Schmidt, G.; Veit, P.; Christen, J.; Wang, X. Q., Color-Tunable 3D InGaN/GaN Multi-Quantum-Well Light-Emitting-Diode Based on Microfacet Emission and Programmable Driving Power Supply. *Adv Opt Mater* **2021,** *9*, 2001400.
11. Zhang, H.; Su, Q.; Chen, S. M., Quantum-dot and organic hybrid tandem light-emitting diodes with multi-functionality of full-color-tunability and white-light-emission. *Nat Commun* **2020,** *11*, 2826.
12. Zhang, W.; Li, H. Z.; Elezzabi, A. Y., Electrochromic Displays Having Two-Dimensional CIE Color Space Tunability. *Adv Funct Mater* **2022,** *32*, 2108341.

13. Zhang, X.; Pan, T.; Zhang, J. X.; Zhang, L. T.; Liu, S. H.; Xie, W. F., Color-Tunable, Spectra-Stable Flexible White Top-Emitting Organic Light-Emitting Devices Based on Alternating Current Driven and Dual-Microcavity Technology. *Acs Photonics* **2019,** *6*, 2350.
14. Cho, K. S.; Lee, E. K.; Joo, W. J.; Jang, E.; Kim, T. H.; Lee, S. J.; Kwon, S. J.; Han, J. Y.; Kim, B. K.; Choi, B. L.; Kim, J. M., High-performance crosslinked colloidal quantum-dot light-emitting diodes. *Nat Photonics* **2009,** *3*, 341.
15. Qian, L.; Zheng, Y.; Xue, J. G.; Holloway, P. H., Stable and efficient quantum-dot light-emitting diodes based on solution-processed multilayer structures. *Nat Photonics* **2011,** *5*, 543.
16. Kwak, J.; Bae, W. K.; Lee, D.; Park, I.; Lim, J.; Park, M.; Cho, H.; Woo, H.; Yoon, D. Y.; Char, K.; Lee, S.; Lee, C., Bright and Efficient Full-Color Colloidal Quantum Dot Light-Emitting Diodes Using an Inverted Device Structure. *Nano Lett* **2012,** *12*, 2362.
17. Liu, M. X.; Yazdani, N.; Yarema, M.; Jansen, M.; Wood, V.; Sargent, E. H., Colloidal quantum dot electronics. *Nat Electron* **2021,** *4*, 548.
18. Dong, Y. T.; Wang, Y. K.; Yuan, F. L.; Johnston, A.; Liu, Y.; Ma, D. X.; Choi, M. J.; Chen, B.; Chekini, M.; Baek, S. W.; Sagar, L. K.; Fan, J.; Hou, Y.; Wu, M. J.; Lee, S.; Sun, B.; Hoogland, S.; Quintero-Bermudez, R.; Ebe, H.; Todorovic, P.; Dinic, F.; Li, P. C.; Kung, H. T.; Saidaminov, M. I.; Kumacheva, E.; Spiecker, E.; Liao, L. S.; Voznyy, O.; Lu, Z. H.; Sargent, E. H., Bipolar-shell resurfacing for blue LEDs based on strongly confined perovskite quantum dots. *Nat Nanotechnol* **2020,** *15*, 668.
19. Liu, Z. J.; Lin, C. H.; Hyun, B. R.; Sher, C. W.; Lv, Z. J.; Luo, B. Q.; Jiang, F. L.; Wu, T.; Ho, C. H.; Kuo, H. C.; He, J. H., Micro-light-emitting diodes with quantum dots in display technology. *Light-Sci Appl* **2020,** *9*, 83.
20. Jang, E.; Kim, Y.; Won, Y. H.; Jang, H.; Choi, S. M., Environmentally Friendly InP-Based Quantum Dots for Efficient Wide Color Gamut Displays. *Acs Energy Lett* **2020,** *5*, 1316.
21. Lutich, A. A.; Mauser, C.; Da Como, E.; Huang, J.; Vaneski, A.; Talapin, D. V.; Rogach, A. L.; Feldmann, J., Multiexcitonic Dual Emission in CdSe/CdS Tetrapods and Nanorods. *Nano Lett* **2010,** *10*, 4646.
22. Wong, J. I.; Mishra, N.; Xing, G. C.; Li, M. J.; Chakrabortty, S.; Sum, T. C.; Shi, Y. M.; Chan, Y. T.; Yang, H. Y., Dual Wavelength Electroluminescence from CdSe/CdS Tetrapods. *Acs Nano* **2014,** *8*, 2873.
23. Galland, C.; Brovelli, S.; Bae, W. K.; Padilha, L. A.; Meinardi, F.; Klimov, V. I., Dynamic Hole Blockade Yields Two-Color Quantum and Classical Light from Dot-in-Bulk Nanocrystals. *Nano Lett* **2013,** *13*, 321.
24. Brovelli, S.; Bae, W. K.; Galland, C.; Giovanella, U.; Meinardi, F.; Klimov, V. I., Dual-Color Electroluminescence from Dot-in-Bulk Nanocrystals. *Nano Lett* **2014,** *14*, 486.
25. Wu, W. Y.; Li, M. J.; Lian, J.; Wu, X. Y.; Yeow, E. K. L.; Jhon, M. H.; Chan, Y. T., Efficient Color-Tunable Multiexcitonic Dual Wavelength Emission from Type II Semiconductor Tetrapods. *Acs Nano* **2014,** *8*, 9349.

26. Gao, Y.; Li, M. J.; Delikanli, S.; Zheng, H. Y.; Liu, B. Q.; Dang, C.; Sum, T. C.; Demir, H. V., Low-threshold lasing from colloidal CdSe/CdSeTe core/alloyed-crown type-II heteronanoplatelets. *Nanoscale* **2018,** *10* (20), 9466-9475.
27. Tarasek, S.; Chou, W. C.; Fan, W. C.; Thomay, T., Excitation power dependent Coulomb induced recombination dynamics in magnetically doped type-II quantum dots. *Nano Express* **2020,** *1*, 010024.
28. Liu, Q.; Derksen, S.; Linder, A.; Scheffer, F.; Prost, W.; Tegude, F. J., Evidence of Type-Ii Band Alignment at the Ordered Gainp to Gaas Heterointerface. *J Appl Phys* **1995,** *77*, 1154.
29. Sun, C. K.; Wang, G.; Bowers, J. E.; Brar, B.; Blank, H. R.; Kroemer, H.; Pilkuhn, M. H., Optical investigations of the dynamic behavior of GaSb/GaAs quantum dots. *Appl Phys Lett* **1996,** *68* (11), 1543-1545.
30. Lim, J.; Park, M.; Bae, W. K.; Lee, D.; Lee, S.; Lee, C.; Char, K., Highly Efficient Cadmium-Free Quantum Dot Light-Emitting Diodes Enabled by the Direct Formation of Excitons within InP@ZnSeS Quantum Dots. *Acs Nano* **2013,** *7*, 9019.
31. Mashford, B. S.; Stevenson, M.; Popovic, Z.; Hamilton, C.; Zhou, Z. Q.; Breen, C.; Steckel, J.; Bulovic, V.; Bawendi, M.; Coe-Sullivan, S.; Kazlas, P. T., High-efficiency quantum-dot light-emitting devices with enhanced charge injection. *Nat Photonics* **2013,** *7*, 407.
32. Etori, H.; Yasuda, T.; Jin, X. L.; Fujita, K.; Mataka, S.; Tsutsui, T., Design of multilayer structure for UV organic light-emitting diodes based on 2-(2-naphthyl)-9,9'-spirobifluorene. *Jpn J Appl Phys 1* **2007,** *46*, 5071.
33. Park, K.; Deutsch, Z.; Li, J. J.; Oron, D.; Weiss, S., Single Molecule Quantum-Confined Stark Effect Measurements of Semiconductor Nanoparticles at Room Temperature. *Acs Nano* **2012,** *6*, 10013.
34. Rowland, C. E.; Susumu, K.; Stewart, M. H.; Oh, E.; Makinen, A. J.; O'Shaughnessy, T. J.; Kushto, G.; Wolak, M. A.; Erickson, J. S.; Efros, A. L.; Huston, A. L.; Delehanty, J. B., Electric Field Modulation of Semiconductor Quantum Dot Photoluminescence: Insights Into the Design of Robust Voltage-Sensitive Cellular Imaging Probes. *Nano Lett* **2015,** *15*, 6848.
35. Porotnikov, D.; Harankahage, D.; Ellison, C.; Yang, M. R.; Cassidy, J.; Zamkov, M., Photoinduced Rotation of Colloidal Semiconductor Nanocrystals in an Electric Field. *Nano Lett* **2021,** *21*, 4787.

TOC: